CHEMISTRY
A European Journal

A Journal of
ChemPubSoc Europe

Accepted Article

Title: The first triple-decker complex with a carbenium center, [CpCo(μ-C3B2Me5)RuC5Me4CH2]+: synthesis, reactivity, X-ray structure and bonding

Authors: Alexander S. Romanov, Dmitry V Muratov, Maddalena Corsini, Alexander R Kudinov, Fabrizia Fabrizi de Biani, and Walter Siebert

To be cited as: *Chem. Eur. J.* 10.1002/chem.201702571

Link to VoR: http://dx.doi.org/10.1002/chem.201702571

Supported by
ACES

WILEY-VCH

The first triple-decker complex with a carbenium center, [CpCo(μ-$C_3B_2Me_5$)$RuC_5Me_4CH_2$]$^+$: synthesis, reactivity, X-ray structure and bonding

Dmitry V. Muratov,*[a] Alexander S. Romanov, *[a] Maddalena Corsini,[b] Alexander R. Kudinov,[a] Fabrizia Fabrizi de Biani,*[b] Walter Siebert*[c]

[a] Institute of Organoelement Compounds, Russian Academy of Sciences, 119991 Moscow, Russian Federation

[b] Dipartimento di Biotecnologie, Chimica e Farmacia, Università di Siena, 53100 Siena, Italy

[c] Anorganisch-Chemisches Institut der Universität Heidelberg, 69120 Heidelberg, Germany

Keywords: Boron, Cobalt, Ruthenium, Electrochemistry, Triple-decker complex, Sandwich compound

ABSTRACT:

The first derivative of the methylium cation with the triple-decker substituent [CpCo($C_3B_2Me_5$)$RuC_5Me_4CH_2$]PF_6 (**2**PF_6), was synthesized from the reaction of the triple decker complex CpCo($C_3B_2Me_5$)RuCp* (**1**) with the salt of the trityl cation [CPh_3]$^+$. The X-ray crystal structure of **2**PF_6 reveals that the methylium carbon is bound to the ruthenium with Ru–C bond length 2.259 Å and corresponds to the description of its structure as η^6-fulvene-ruthenium. Reactions of **2**PF_6 with nucleophiles OH^-, Ph_3P, Et_3N led to the corresponding derivatives of **1** in high yields. Aromatic amines $PhNEt_2$ and 4-$MeC_6H_4NH_2$ react with **2**PF_6 to give the electrophilic aromatic substitution products quantitatively. Chemical reduction of **2**PF_6 with Zn powder in tetrahydrofuran leads to the formation of the bis(triple-decker) derivative ($CpCo(C_3B_2Me_5)RuC_5Me_4CH_2)_2$ (**10**) with a CH_2CH_2-bridge. The structures of complexes **4**, **5**, **7**–**10** were determined by X-ray diffraction. Density functional calculations support the crystallographically determined geometry of **2** and allow rationalization of some characteristics of its structure, spectroscopy, and reactivity.

Introduction

The methylium cation $[CH_3]^+$ is very unstable and was detected only in the gas phase.[1] It is well established that certain substituents can effectively stabilize this cation. For instance, Olah et al. observed the tert-butyl carbocation $[CMe_3]^+$ by multinuclear NMR (^1H, ^2H, ^{13}C and ^{19}F) as a stable species on dissolving tert-butyl fluoride in SbF_5/SO_2 system at room temperature.[2] An even greater stabilizing effect is shown by groups capable for π-conjugation (e.g., $CH=CH_2$, Ph, NR_2).[3] In particular, the salts of the trityl cation $[CPh_3]^+$ are stable enough to be stored in inert atmosphere for a long time.

The carbenium ions can be also stabilized due to coordination with transition metals Examples of such stabilization have been reported for the mononuclear η^5 cyclobutadienylmethylium $[(\eta^5\text{-}C_4H_3CH_2)Fe(CO)_3]^+$ [4] and η^7-benzylium $(\eta^7\text{-}C_6H_5CH_2)Cr(CO)_3]^+$ complexes,[5] as well as the di- and polynuclear complexe $[Co_2(CO)_6(HC{\equiv}CCH_2)]^+$,[6] $[Mo_2Cp_2(CO)_4(HC{\equiv}CCH_2)]^+$ [7] or $[Co_3(CO)_9(\mu_3\text{-}CCH_2)]^+$.[8]

The most well-known are α-metallocenylmethylium ions, e.g. $[CpFe(C_5H_4CH_2)]^+$.[9] Synthesis, reactivity, stereochemistry, structures, and bonding features of such complexes hav been extensively studied.[10] Ruthenocenyl and osmocenyl analogs have been also prepared. Fo instance, Barlow et al. described the parent ruthenocenylmethylium cation $[CpRuC_5H_4CH_2]^+$, it reactivity, redox properties and X-ray structure.[11] The mechanism of stabilization of th carbenium center in such complexes was extensively discussed. According to extende Hückel[12] and DFT calculations,[11] the stabilization occurs due to predominant contribution o the structure with η^6-coordinated fulvene ligand (Chart 1).

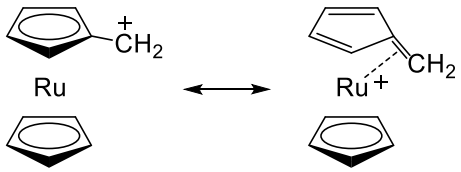

Chart 1

Since 1980, Siebert et al. described a number of μ-diborolyl triple-decker complexes.[13] Using electrophilic stacking reactions of the sandwich anion $[CpCo(C_3B_2Me_5)]^-$ with half sandwich cations we prepared both neutral[14] and cationic[15] complexes of this type. Herein w report the synthesis and reactivity of the first triple-decker-substituted methylium cation $[CpCo(C_3B_2Me_5)RuC_5Me_4CH_2]^+$. The mechanism of its stabilization was elucidated based on X-ray diffraction and DFT calculations.

Results and Discussion

10.1002/chem.201702571

Synthesis and Reactivity

Recently, we have synthesized the μ-diborolyl triple-decker complex $CpCo(C_3B_2Me_5)RuCp^*$ (**1**) by reaction of the sandwich anion $[CpCo(C_3B_2Me_5)]^-$ with $[Cp^*Ru(MeCN)_3]^+$.[14] In the present work we found that treatment of the blue compound **1** with the trityl cation affords red cationic complex $[CpCo(C_3B_2Me_5)Ru(C_5Me_4CH_2)]^+$ (**2**) in 90% yield (Scheme 1).

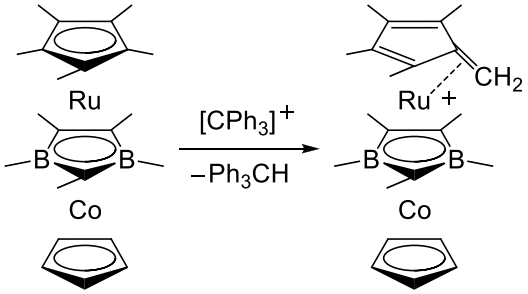

1 **2**

Scheme 1. Preparation of the cationic complex $[CpCo(C_3B_2Me_5)Ru(C_5Me_4CH_2)]^+$ (**2**).

In a similar manner, Köelle et al. have prepared the related nonamethylruthenocenylmethylium cation $[Cp^*RuC_5Me_4CH_2]^+$ (**3**, Chart 2)[16],[17] by reaction of decamethylruthenocene with $[CPh_3]^+$. It should be noted however that the analogous reaction of 1,1′-dimethylruthenocene failed to give the (1′-methylruthenocenyl)methylium cation,[11] suggesting its lower stability.

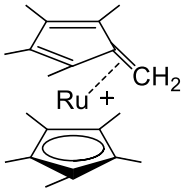

3

Chart 2

The ^1H and ^{13}C NMR signals of the CH_2 group in **2** are observed at 4.55 and 76.2 ppm respectively, which is characteristic for sp^2-carbon. For the related cation **3** values 4.75 and 77.1 ppm were observed.[16b]

The hexafluorophosphate salt of the cation **2** is air-stable both in the solid state and in solutions in aprotic solvents, indicating high stabilization of the carbenium-center. Nevertheless, the cation **2** is sensitive to attack by strong nucleophiles. For instance, the reaction with aqueous KOH affords the triple-decker alcohol **4** (Scheme 2). Cation **2** also reacts with PPh_3 giving the phosphonium salt **5**. Both reactions proceed with a color change from red to blue.

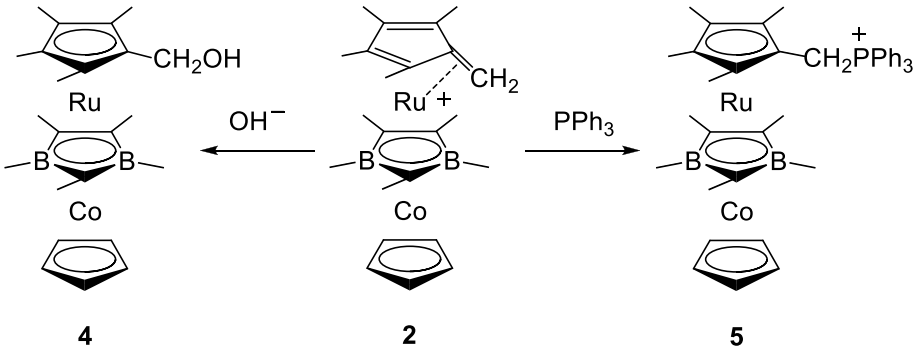

Scheme 2. Reactivity of the cation **2** with nucleophiles.

Similar reaction with the aliphatic amine NEt_3 primarily gives the ammonium salt (identified by ^1H NMR spectra). This salt slowly reacts with traces of water giving ether bearing two triple-decker moieties (Scheme 3).

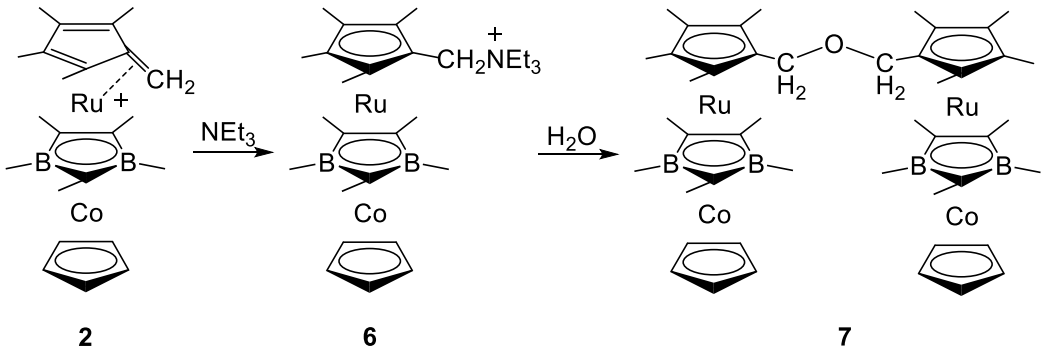

Scheme 3. Reactivity of the cation **2** with nucleophiles.

Interestingly, the reactions of **2** with aromatic amines occur in a different way. Fo instance, the reaction with N,N-diethylaniline (1 eq, Scheme 4) leads to the cationic complex as a result of electrophilic substitution in *para*-position of the phenyl group. Similar reactio with an excess of *p*-toluidine proceeds in *ortho*-position (since the *para*-position is occupied giving the neutral complex **9**; the reaction is accompanied by deprotonation.

We found that the nonamethylruthenocenylmethylium cation **3** also gives the products o the electrophilic substitution with aromatic amines.[18] According to ^1H NMR, in the reaction of cations **2** and **3** with $PhNEt_2$ the full conversion into products was achieved after 8 and 24 h, respectively. One may conclude that slower consumption of the triple-decker cation **2** indicates the higher stabilization of the carbenium-center compared to metallocene analog **3**.

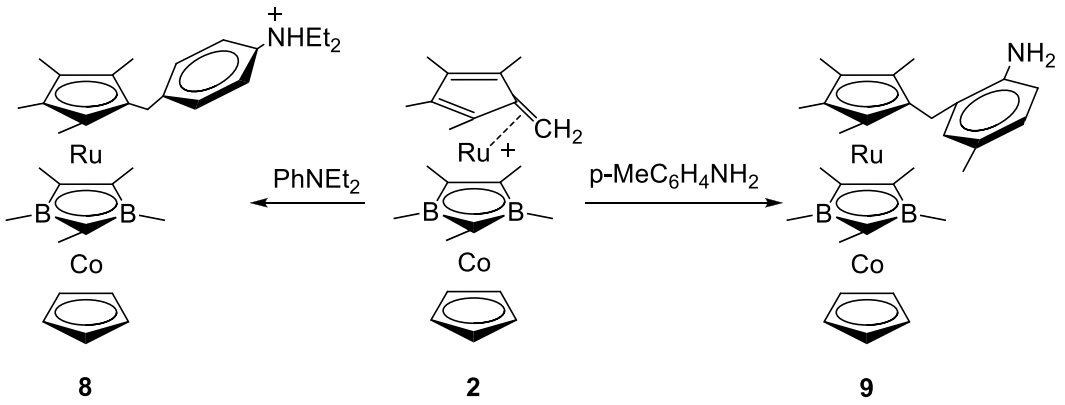

Scheme 4. Reactivity of the cation **2** with aromatic amines.

The reduction of **2** with an excess of Zn powder in THF gives complex **10** having a CH_2CH_2 bridge between two triple-decker moieties (Scheme 5).

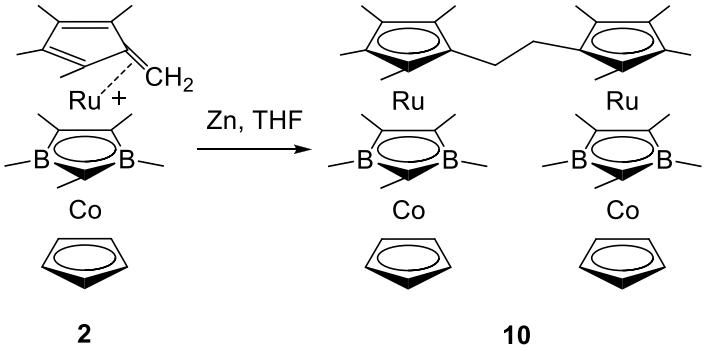

Scheme 5. Chemical reduction of the cation **2**.

X-Ray diffraction study

Structures of the triple-decker complexes **2**PF_6, **4**, **7**, **8**PF_6, **9**, and **10** were determined by X-ray diffraction (for the selected bond lengths and angles see Tables S1, S2 in the Supporting Information). In the case of **2**PF_6 (the structure of cation is shown on Figure 1) three independent molecules are present in the unit cell; average values are discussed below. The conformation of the C_3B_2 and C_5(Ru) rings is pseudo-eclipsed for the independent molecules A and B (C–H···F and C–H···π intermolecular contacts), and staggered for the independent molecule C (only C-H···F intermolecular contacts). Complexes **4**, **7**, and **8**PF_6 possess a pseudo-eclipsed conformation for the C_3B_2 and C_5(Ru) rings while it is staggered for complexes **9** and **10**. Presence of the both conformations indicates that the energy barrier between them is low and largely depends on the intermolecular contacts. This was previously discussed for the ruthenium-type sandwich complexes.[19]

The planes of C_5(Co) and C_3B_2 ring ligands are almost parallel (the dihedral angle 1.4°). However, the C_3B_2 and C_5(Ru) rings are tilted by 7.3° (cf. 6.8° for **3**BPh_4)[16c]. The angle

10.1002/chem.201702571

between the C_5(Ru) ring centroid and the C–CH_2 (C14–C19) bond (40.1°) is greater than the corresponding angle in **3** (39.4°). The Ru–CH_2 distance in **2** (2.259(6) Å) is slightly shorter than that in **3** (2.270(3) Å) suggesting stronger bonding.

The C–CH_2 bond (1.394(8) Å) is much shorter than C–CH_3 bonds for C_5(Ru) ring (1.489–1.515, av 1.503(8) Å) suggesting its double-bond character. The C15–C16 and C17–C18 bonds (av 1.398(9) Å) are considerably shorter than C14–C15, C14–C18 (av 1.460(9) Å) and C16–C17 (1.425(9) Å) indicating bond alternation. In overall, the structural data suggest fulvene-type bonding of the $C_5Me_4CH_2$ ligand.

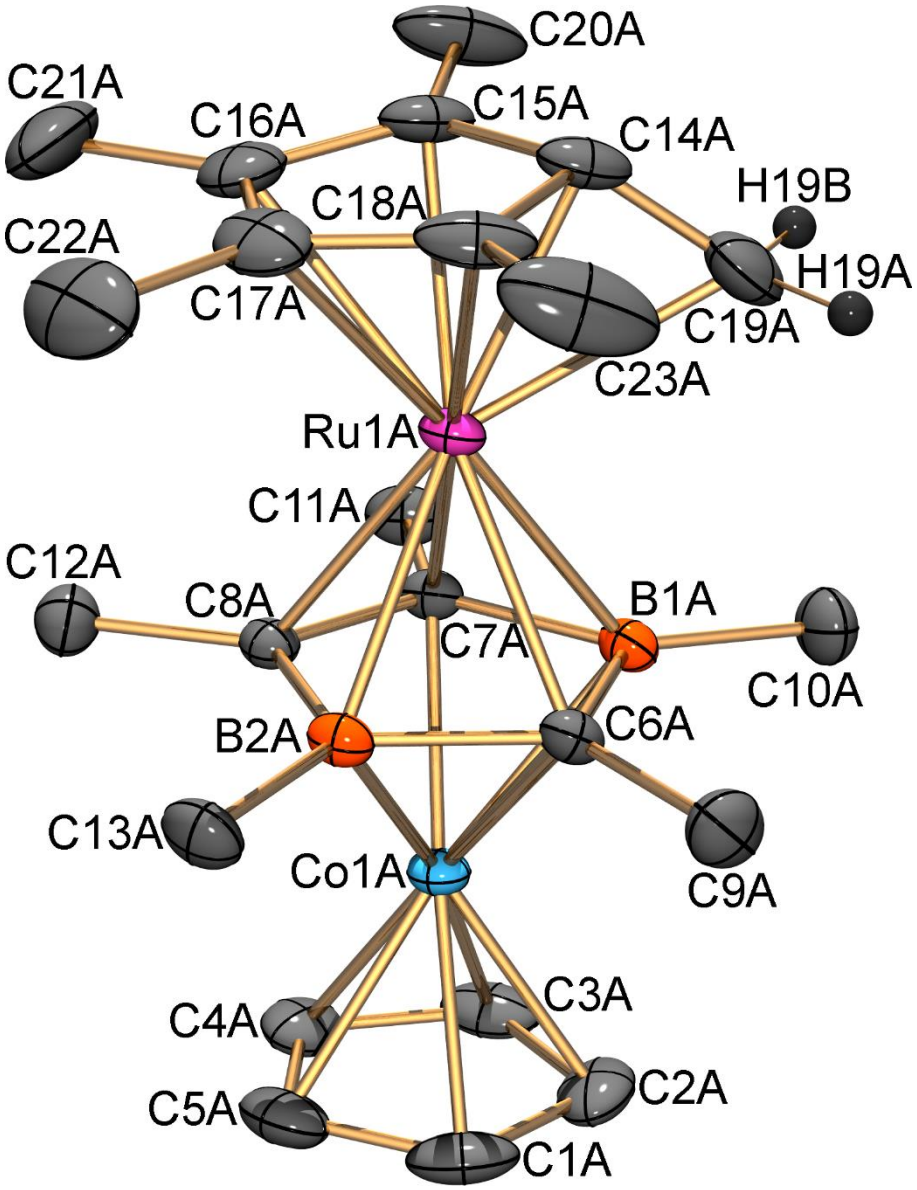

Figure 1. The structure of the cation **2**. Ellipsoids are shown at the 30% level. All hydrogen atoms except for CH_2 are omitted for clarity.

The structure of alcohol **4** is shown on Figure 2. In contrast to **2** the CH_2 group in **4** does not interact with the Ru center. Cross-orientation of all five-membered rings in **4** is perfectly

10.1002/chem.201702571

eclipsed. The planes of all ring ligands are almost parallel, the dihedral angles Cp/C_3B_2 and C_3B_2/C_5(Ru) being 1.6° and 1.7°, respectively. The atom C19 is bent slightly away from the C_5 plane, elongating distance Ru···C19 to 3.277(6) Å. There is no C–C noticeable bond alternation within $C_5Me_4CH_2OH$ ligand. The metal-to-ring distances Co···Cp (1.658 Å), Co···C_3B_2 (1.581 Å), Ru···C_3B_2 (1.793 Å), and Ru···C_5 (1.789 Å) are similar to those in **1** (1.654, 1.590, 1.776, and 1.788 Å, respectively).[14] The molecules **4** in the crystal are arranged along 4_1 axis due to formation of intermolecular hydrogen bonds O(1)–H(1)···O(1)$_{-0.75+y,\ 1.25-x,\ 0.25+z}$ (with r(O–O) = 2.695(2) Å and O–H–O angle = 170(3)º).

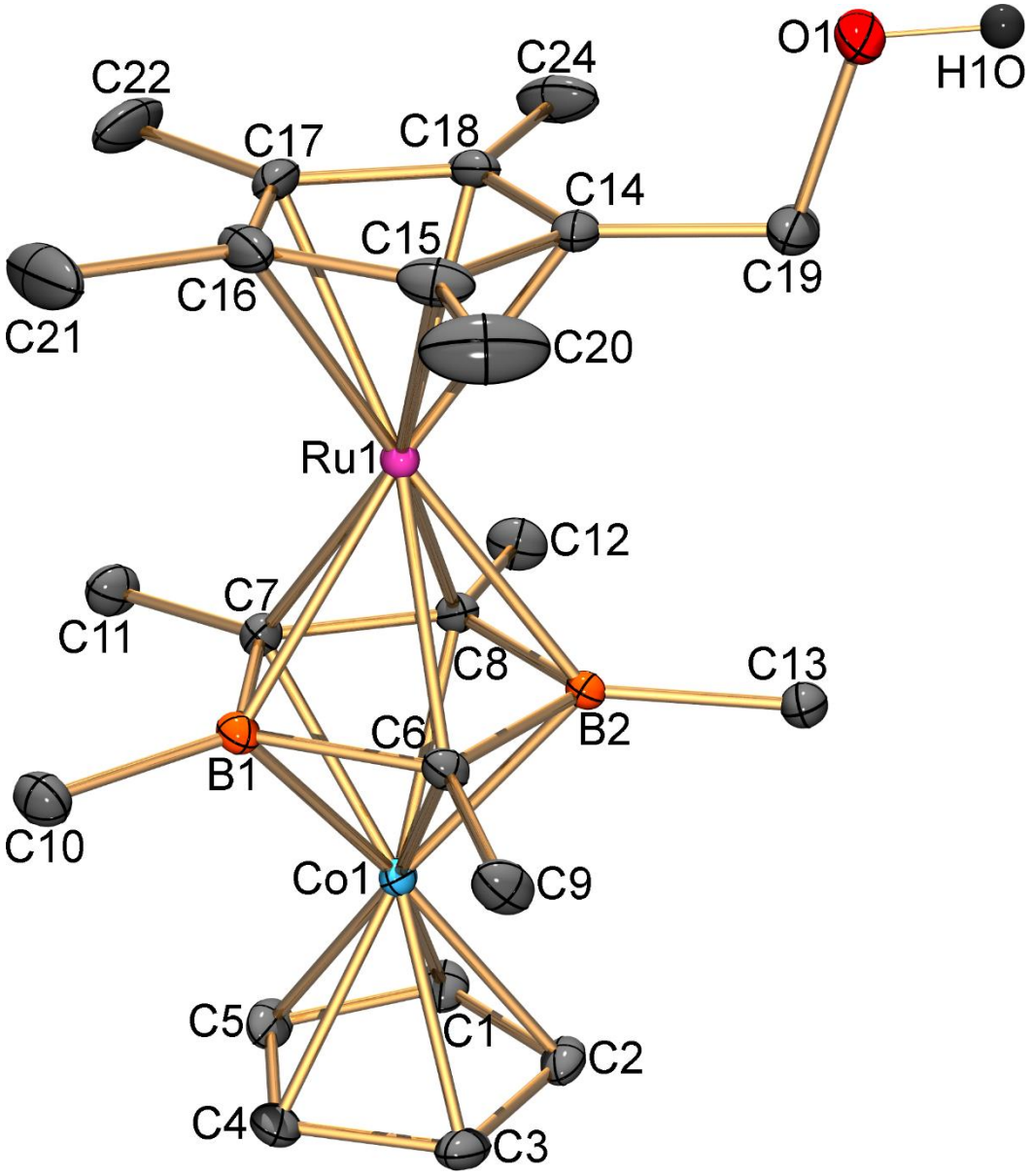

Figure 2. Molecular structure of the complex **4**. Ellipsoids are shown at the 30% level. All hydrogen atoms except for OH are omitted for clarity.

10.1002/chem.201702571

The structures of complexes **7**–**10** are shown on Figures 3–6. All these compounds can be considered as organic derivatives of triple-decker complex $CpCo(\mu\text{-}C_3B_2Me_5)RuCp^*$ (**1**) having similar structures. The planes of all ring ligands are almost parallel, the dihedral angles Cp/C_3B_2 and C_3B_2/C_5(Ru) are within the range 0° to 2.7°. The metal-to-ring distances Co···Cp (1.647 – 1.655 Å), Co···C_3B_2 (1.575 – 1.585 Å), Ru···C_3B_2 (1.773 – 1.788 Å), and Ru···C_5 (1.772 – 1.785 Å) are similar to those in **2** (1.654, 1.590, 1.776, and 1.788 Å, respectively).

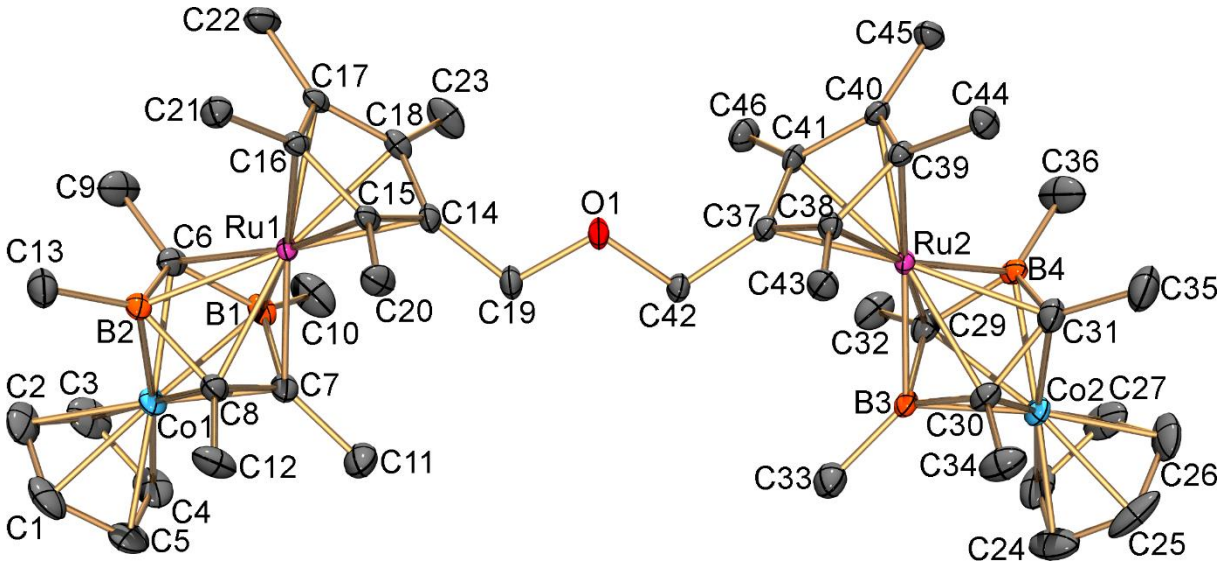

Figure 3. Molecular structure of the complex **7**. Ellipsoids are shown at the 50% level Hydrogen atoms are omitted for clarity.

10.1002/chem.201702571

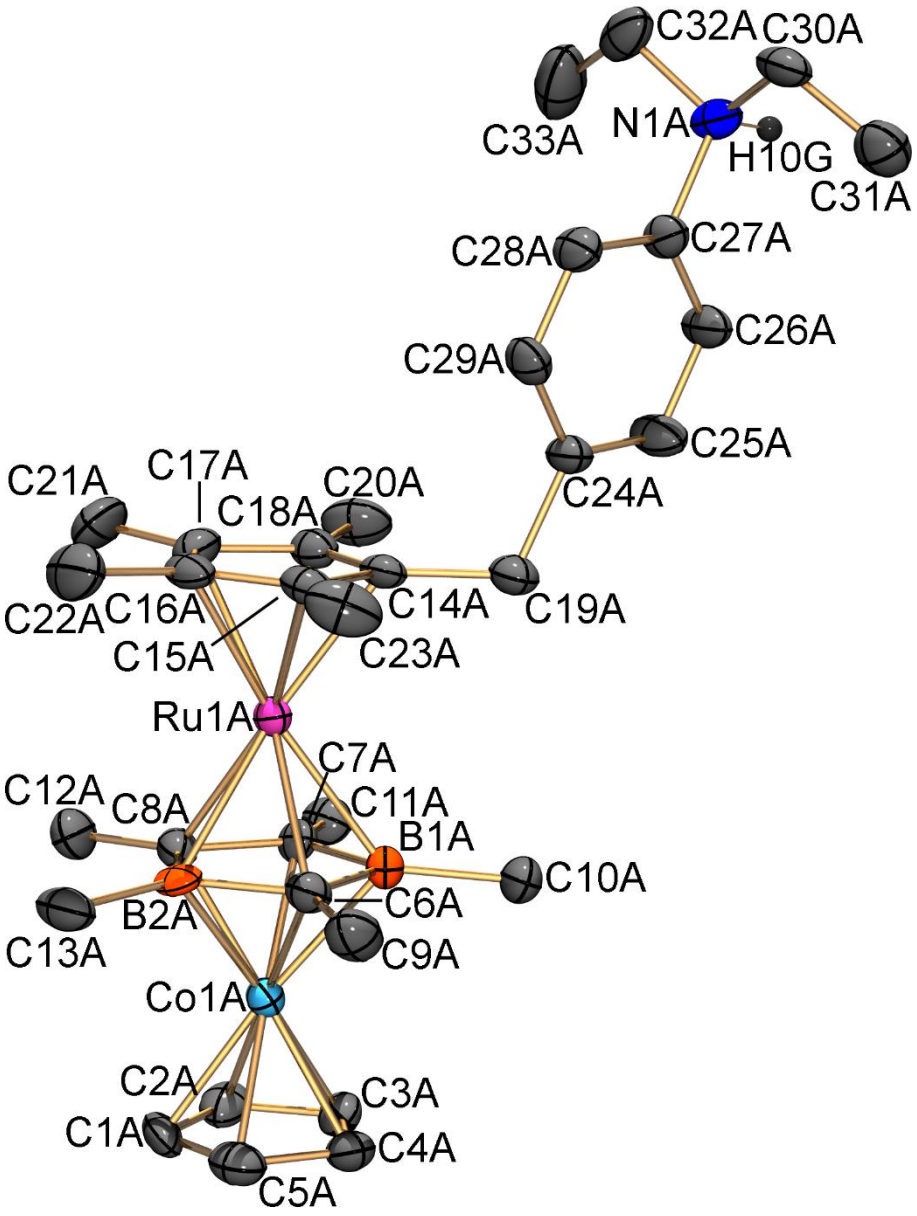

Figure 4. Molecular structure of the cation **8**. Ellipsoids are shown at the 50% level. Al hydrogen atoms except for NH are omitted for clarity.

10.1002/chem.201702571

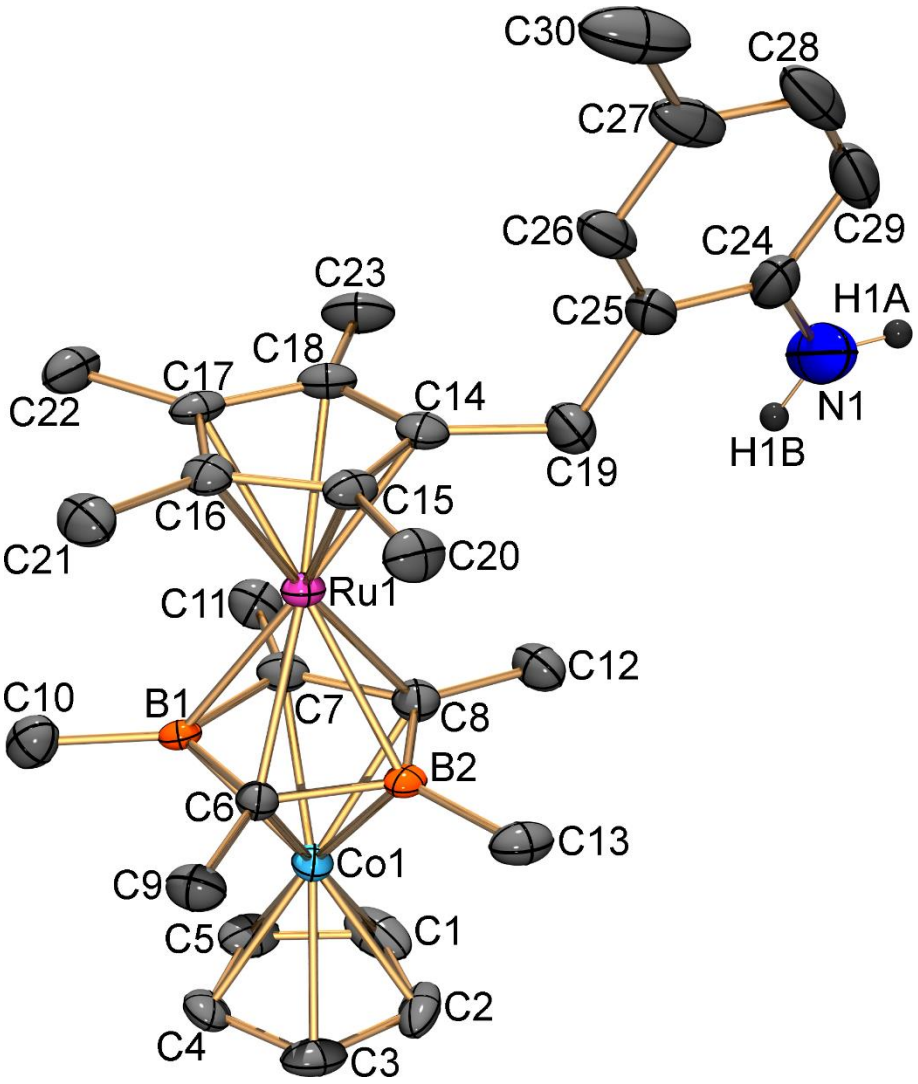

Figure 5. Molecular structure of the complex **9**. Ellipsoids are shown at the 50% level. Al hydrogen atoms except for NH_2 are omitted for clarity.

10.1002/chem.201702571

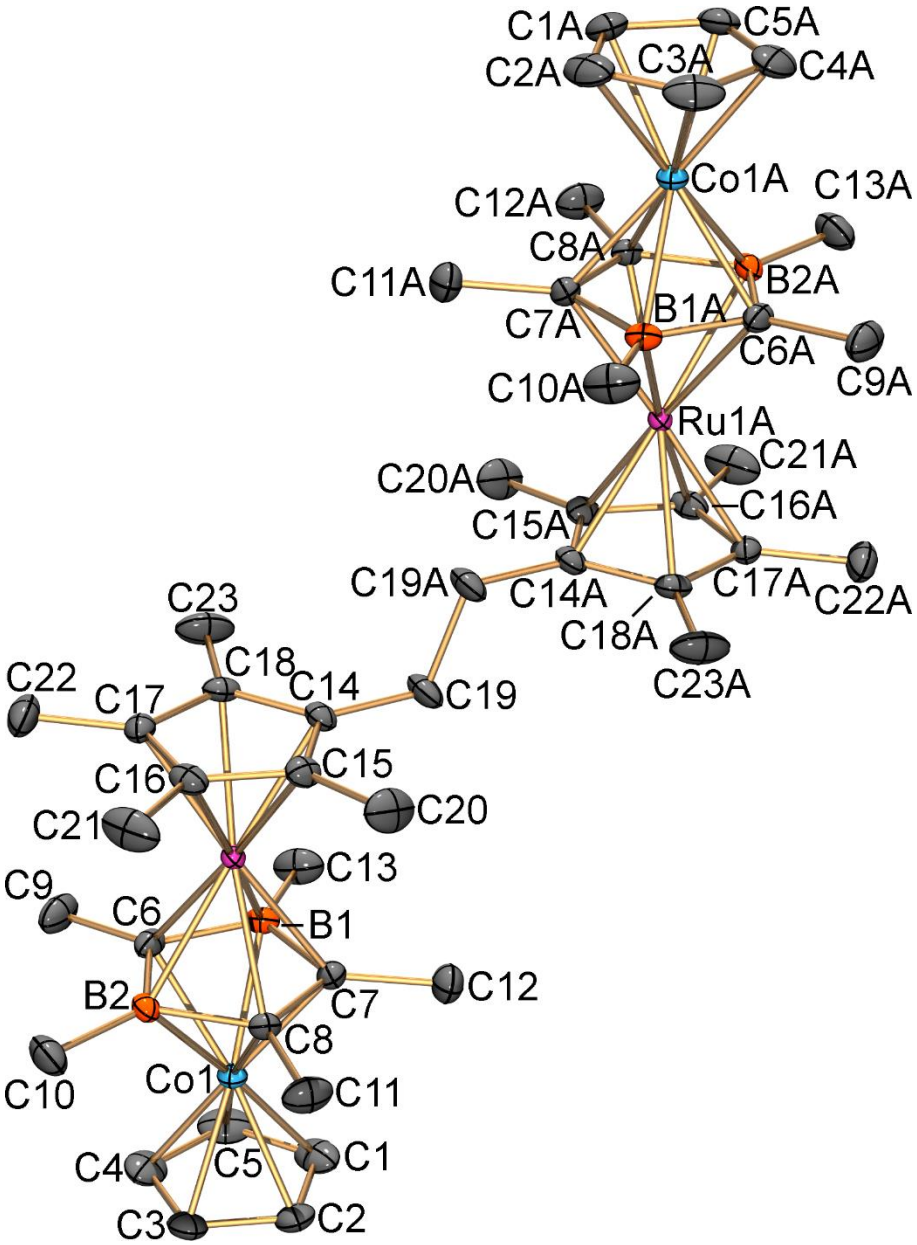

Figure 6. Molecular structure of the complex **10**. Ellipsoids are shown at the 50% level Hydrogen atoms are omitted for clarity. Symmetry code A: 2-x, -y, 2-z.

Electrochemistry and Spectroelectrochemistry[20]

It has been previously shown[11] that the chemical reduction of the paren ruthenocenylmethylium cation $[CpRu(C_5H_4CH_2)]^+$, close analogue to $[\mathbf{3}]^+$, leads to the formation of 1,2-bis(ruthenocenyl)ethane, with bis(ruthenocenylmethyl)ether and methylruthenocene as byproducts. Similarly, we have observed the formation of the dimer $[\mathbf{10}]^0$ as the result of the chemical reduction of $[\mathbf{2}]^+$.

Cyclic voltammetry has proven to be an elegant way to go into details of these dimerization reactions. The redox potential values of $[\mathbf{2}]^+$ and $[\mathbf{3}]^+$ are collected in Table 1,

together with those of dimer [**10**]^0 and the triple-decker complex [**1**]^0, reported for comparison. The cyclic voltammetric profiles of [**2**]$^+$ and [**3**]$^+$ are compared in Figure 7a,b. Here, we put in evidence that in both cases the first anodic scan is flat, indicating that the oxidation of these compounds, if any, is not achievable in the experimental window. On the other side, both compounds undergo an irreversible reduction process (at –1.00 and –1.45 V for [**2**]$^+$ and [**3**]$^+$, respectively), after which a new anodic process appears on the backward scan. The same cyclic voltammetric profile has been obtained both at low (about –20 °C) and room temperature. This behaviour is confirmed by the bulk electrolysis experiments: in fact, the addition of one electron per molecule makes the original compounds to disappear from the solution, while new species are formed, which can be oxidised in a closely-spaced group of anodic processes. In truth, the reduction of [**3**]$^+$ probably generates a mixture of compounds, since more than two, almost overlapping, oxidation processes are visible in the anodic scan of the resulting solution (Figure S1 in the Supporting Information). On the contrary, the reduction of the triple-decker cation [**2**] clearly produces dimer [**10**]^0, as demonstrated by the appearance of two well-shaped successive oxidations at the same potential values as observed in the cyclic voltammetry of a pristine sample of [**10**]^0 (Figure 7c).

The UV-vis spectroelectrochemical experiment (Figure 8) reveals how the step-by-step reduction of a solution of [**2**]$^+$ induces subtle but significant changes of the spectrum: the intensity of the high energy set of bands slightly decreases, while, more meaningfully, the broad and weak lower energy band is red-shifted from 560 to 577 nm. This value perfectly matches that of a pure sample of [**10**]^0. As a net difference (Figure 8, bottom) the spectral component centred at ~510 nm diminishes, while that centred at ~630 nm grows and the originally orange solution of [**2**]$^+$ turns green, which is the colour of the solution of [**10**]^0. Moreover, the spectroelectrochemical experiment further confirms the clean and very fast dimerisation of radical [**2**]^0 to [**10**]^0, since four isosbestic points are persistently visible during the redox-induced spectral changes.

A final comment about the presence of two separate oxidation steps observed in the cyclic voltammetry of [**10**]^0 is also necessary. In fact, the 'monomeric' triple-decker complex [**1**]^0 only exhibits a single oxidation process at +0.25 V and one would not expect the -CH_2CH_2 linker to be able to allow the electronic communications of the two halves in [**10**]^0, which would be at the origin of two separate oxidations as a result of a mixed valence class II regime. Thus, we have also performed the spectroelectrochemistry of [**10**]^0 on oxidation, to counter-check for the presence of an intervalence charge transfer (IT) band in [**10**]$^+$, eventually confirming the class II of [**10**]^0. Anyway, as the spectrum of [**10**]^0 is almost overlapping that of [**1**]^0, the spectrum of [**10**]$^+$ (and that of [**10**]$^{2+}$) also more or less overlaps that of [**1**]$^+$, so indicating that

10.1002/chem.201702571

$[\mathbf{10}]^+$ is a class I mixed valence compound and that, as expected, the saturated linker is unable to open an electronic communication pathway. For both $[\mathbf{1}]^0$ and $[\mathbf{10}]^0$, the removal of one electron makes the band in the visible region (580 and 577 nm for $[\mathbf{1}]^0$ and $[\mathbf{10}]^0$, respectively) to disappear, while a lower energy broad band (888 nm for $[\mathbf{1}]^+$ and 940 nm for $[\mathbf{10}]^+$ and $[\mathbf{10}]^{2+}$) appears. The nature of this low energy band in $[\mathbf{1}]^+$ has been clarified in a previous work[14] and its IT origin has been excluded. On the other side, the absence of additional NIR bands in $[\mathbf{10}]^+$, together with the fact that all the bands monotonically change on passing from $[\mathbf{10}]^0$ to $[\mathbf{10}]^+$ and then to $[\mathbf{10}]^{2+}$, allow to safely state that in the dimer $[\mathbf{10}]^0$ there is no any electronic communication between the two halves. Thus, we can only ascribe the splitting of the two electrons removal in two separate oxidation processes to electrostatic effects.

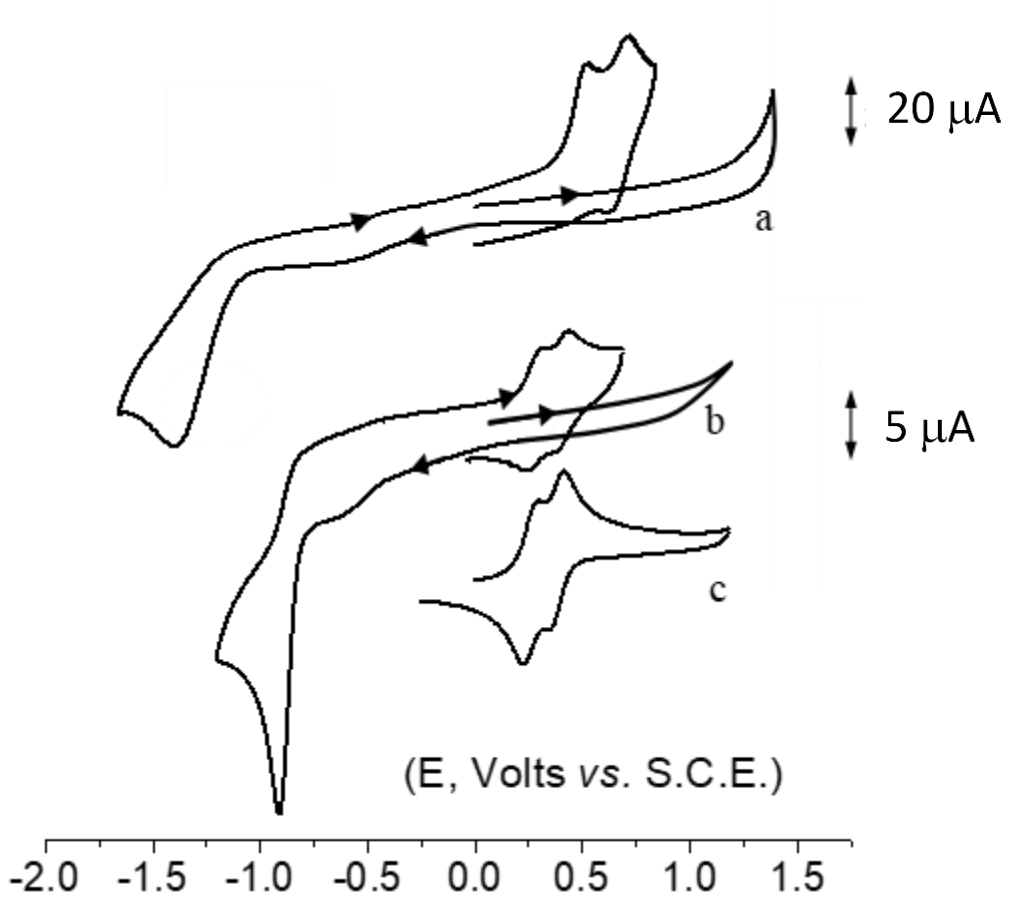

Figure 7. Cyclic voltammetric responses recorded at a platinum electrode in CH_2Cl_2 solutions o (a) $[\mathbf{3}]^+$ (0.8×10^{-3} M); (b) $[\mathbf{2}]^+$ (0.4×10^{-3} M); (c) $[\mathbf{10}]^0$ (0.7×10^{-3} M) $[NBu_4][PF_6]$ (0.2 M) supporting electrolyte. Scan rate 0.2 V s^{-1}. T = 298 K.

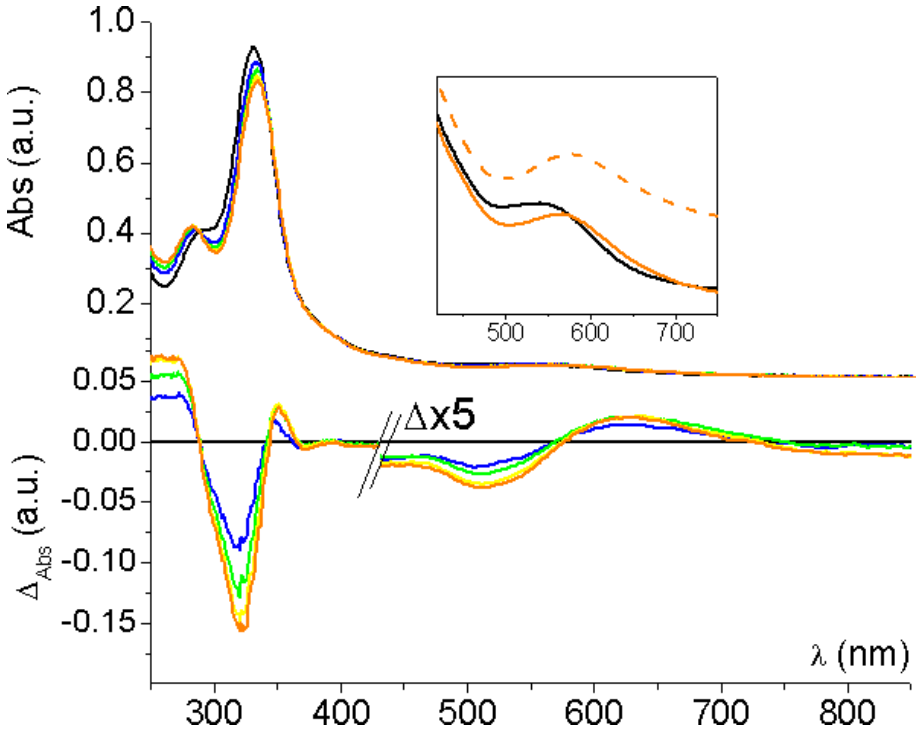

Figure 8. Spectral changes (top) and difference spectra (bottom) recorded in an OTTLE cel upon progressive reduction of $[\mathbf{2}]^+$ in CH_2Cl_2 solution. $[NBu_4][PF_6]$ (0.2 M) supportin electrolyte. Inset: initial (black) and after exhaustive reduction (orange) spectra of $[\mathbf{2}]^+$ compare with the spectrum of $[\mathbf{10}]^0$ (dashed orange). T = 298 K.

Table 1. Formal Electrode Potentials (in V, *vs* SCE) and Peak-to-Peak Separations (in mV) for the Redox Changes Exhibited by the Triple-Decker Complexes under Study in CH_2Cl_2 Solution at T =298 K.

Complex	$E^{0\prime}$ (ΔE_p)		
	reduction	oxidation	
$[\mathbf{2}]^+$	-1.00[b]		
$[\mathbf{3}]^+$	-1.45[a]		
$[\mathbf{10}]^0$ (dimer)	-	+0.28 (80)	+0.40 (80)
$[\mathbf{1}]^0$		+0.25 (90)[c]	

[a] Irreversible. After exhaustive electrolysis on reduction new peaks at +0.28 V and +0.40 V appear; [b] Irreversible. After exhaustive electrolysis on reduction new ill-defined peaks at +0.50 V and +0.70 V appear; [c] From ref. [14].

Theoretical consideration

Let us first compare the parent triple-decker and sandwich complexes $[CpCo(1,3\text{-}C_3B_2H_5)Ru(C_5H_4CH_2)]^+$ (**2'**) and $[CpRu(C_5H_4CH_2)]^+$ (**3'**), which structures were optimized using all-electron scalar-relativistic calculations at PBE/L2 level (Figure 9).[21] Table 2 summarizes Ru–

10.1002/chem.201702571

C and C–C distances and Mayer bond orders (MBO) in the Ru($C_5H_4CH_2$) moiety of these cations. For cation **2'** the Ru–CH_2 distance is shorter and MBO is higher than in **3'**, suggesting stronger interaction of the metal atom with carbenium center, in accordance with X-ray structures for the methylated derivatives **2** and **3** (calculated distances: 2.254 and 2.266 Å, respectively; experimentally observed: 2.259 and 2.270 Å, respectively). Interestingly, for both parent cations MBOs of the Ru–CH_2 bond are substantially higher compared to other Ru–C bonds (inspite of the fact that the respective distance is the longest in the Ru($C_5H_4CH_2$) moiety).

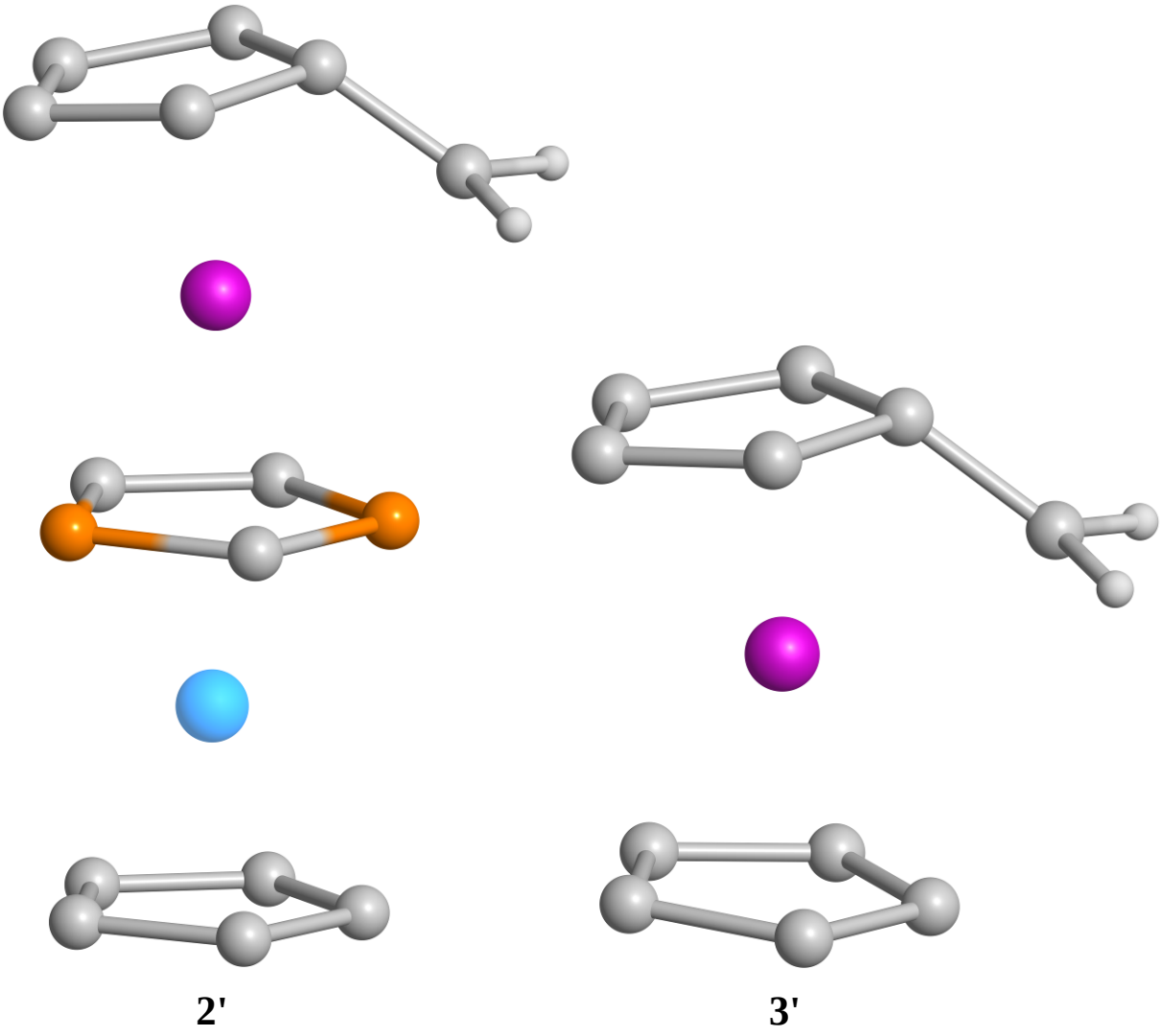

Figure 9. Optimized structures of the parent cations **2'** and **3'** at PBE/L2 level. All hydrogen atoms except for CH_2 are omitted for clarity.

Table 2. Selected Ru–C and C–C distances (Å)[a] and Mayer bond orders (in parentheses)[b] for the parent cations **2'** and **3'**.

10.1002/chem.201702571

Bond	**2'**	**3'**
Ru–CH_2	2.274 (0.63)	2.287 (0.62)
Ru–C_{ipso}	2.078 (0.46)	2.078 (0.47)
Ru–C_α	2.179 (0.59)[c]	2.187 (0.56)
Ru–C_β	2.247 (0.48)[c]	2.256 (0.47)
C_{ipso}–CH_2	1.415 (1.20)	1.413 (1.19)
C_{ipso}–C_α	1.465 (1.04)[c]	1.465 (1.03)
C_α–C_β	1.418 (1.19)[c]	1.417 (1.21)
C_β–C_β	1.439 (1.12)	1.440 (1.11)

[a] At PBE/L2. [b] At BP86/def2-TZVPP. [c] Average values.

The C_{ipso}–CH_2 bond in **2'** and **3'** is shorter than other C–C bonds in the $C_5H_4CH_2$ moiety The MBO values for this bond (1.2) suggest its partial double-bond character. Respectively, th bond alternation in the C_5 ring is observed. In particular, the C_α–C_β bond is the shortest (bon order 1.2) whereas the C_{ipso}–C_α is the longest (1.0); the C_β–C_β bond holds an intermediat position (1.1). In both complexes the C_{CH2} atom is only slightly deviated (by 0.128 and 0.129 Å respectively) from the C_{ipso}/H1/H2 plane, indicating a classical π bonding with the metal.

The partial double-bond character of C_{ipso}–CH_2, C_α–C_β, and C_β–C_β bonds is als supported by frontier orbitals of the unsubstituted fulvene fragment $C_5H_4CH_2$ with the geometr it has in the parent complex $[CpCo(C_3B_2H_5)RuC_5H_4CH_2]^+$ (Figure S2 in the Supportin Information). Indeed, HOMO and HOMO–1 are essentially π-orbitals. These orbitals ar responsible for π donation $C_5H_4CH_2 \rightarrow [CpCo(C_3B_2H_5)Ru]^+$, whereas LUMO and LUMO+ participate in δ back donation $[CpCo(C_3B_2H_5)Ru]^+ \rightarrow C_5H_4CH_2$. Noteworthy, both HOMO– and LUMO have considerable contribution of the p orbital of the CH_2 carbon atom.

In order to evaluate the substitution effect on the stability of the methylium cation CH_3^+ the stabilization energies for selected substituents (H, Me, Ph, NH_2, NMe_2, $CpRuC_5H_4$, $Cp^*RuC_5Me_4$, $CpCo(C_3B_2H_5)RuC_5H_4$, $CpCo(C_3B_2Me_5)RuC_5Me_4$ were calculated in accordance with the reaction $CH_3^+ + RCH_3 \rightarrow CH_4 + RCH_2^+ + \Delta E_{stab}$ (Table 3). As seen, the stabilizing effect of the unsubstituted ruthenocenyl substituent is greater than those of Ph and NR_2 (R = H, Me) groups. However, this effect is smaller than that of three Ph groups, explaining failure of the preparation of the parent cation **3'** by reaction of methylruthenocene with trityl cation.[11]

Nevertheless, the stabilizing effect of nonamethylated ruthenocenyl substituent is considerably greater than that of Ph_3 explaining easy preparation of cation **3** by hydride abstraction from $RuCp^*_2$ with $[CPh_3]^+$.[16a]

Interestingly, the stabilizing effect of the parent triple-decker substituent $CpCo(C_3B_2H_5)RuC_5H_4$ is 10 kcal mol^{-1} greater than that of $CpRuC_5H_4$. Nonamethylation results in additional stabilization (by 12 kcal mol^{-1}), however the latter effect is smaller than in the case of ruthenocenyl (19 kcal mol^{-1}). As a result (or in overall), the stabilizing effect of the methylated triple-decker substituent $CpCo(C_3B_2Me_5)RuC_5Me_4$ is 2.5 kcal mol^{-1} greater than that of $Cp^*RuC_5Me_4$. It may be concluded that the triple-decker substituent used in this work possesses a record stabilization of the methylium cation. It correlates with the stronger Ru–CH bonding in cations **2** and **2'** compared to **3** and **3'** (vide supra). In full accordance with these data the CH_2 carbon atom has the greatest negative electrostatic potential E_C among the studied substituents (last column in Table 3).

Table 3. Stabilization energies ΔE_{stab} (in kcal mol^{-1}) and electrostatic potentials of the key carbon atom E_C at BP86/TZ2P level.

Substituent	ΔE_{stab} [a]	E_C
H	0 (0)	-14.349
CH_3	-48.95 (-48.33)	-14.471
Ph	-84.52 (-83.37)	-14.552
NH_2	-100.82 (-104.83)	-14.454
NMe_2	-120.36 (-121.12)	-14.516
$CpRuC_5H_4$	-121.28 (-122.01)	-14.610
$Cp^*RuC_5Me_4$	-140.60 (-141.30)	-14.651
$CpCo(C_3B_2H_5)RuC_5H_4$	-131.29 (-132.07)	-14.632
$CpCo(C_3B_2Me_5)RuC_5Me_4$	-143.14 (-144.01)	-14.657
Ph_3	-126.82 (-126.29)	-14.593

[a] Values at PBE/L2 are given in parentheses.

Figure 10 illustrates LUMOs of the the parent cations **2'** and **3'**. The LUMO coefficient on the CH_2 carbon atom for the triple-decker complex **2'** is much smaller than for the mononuclear analog **3'**, suggesting lower electrophilicity of **2'** compared with **3'**.

10.1002/chem.201702571

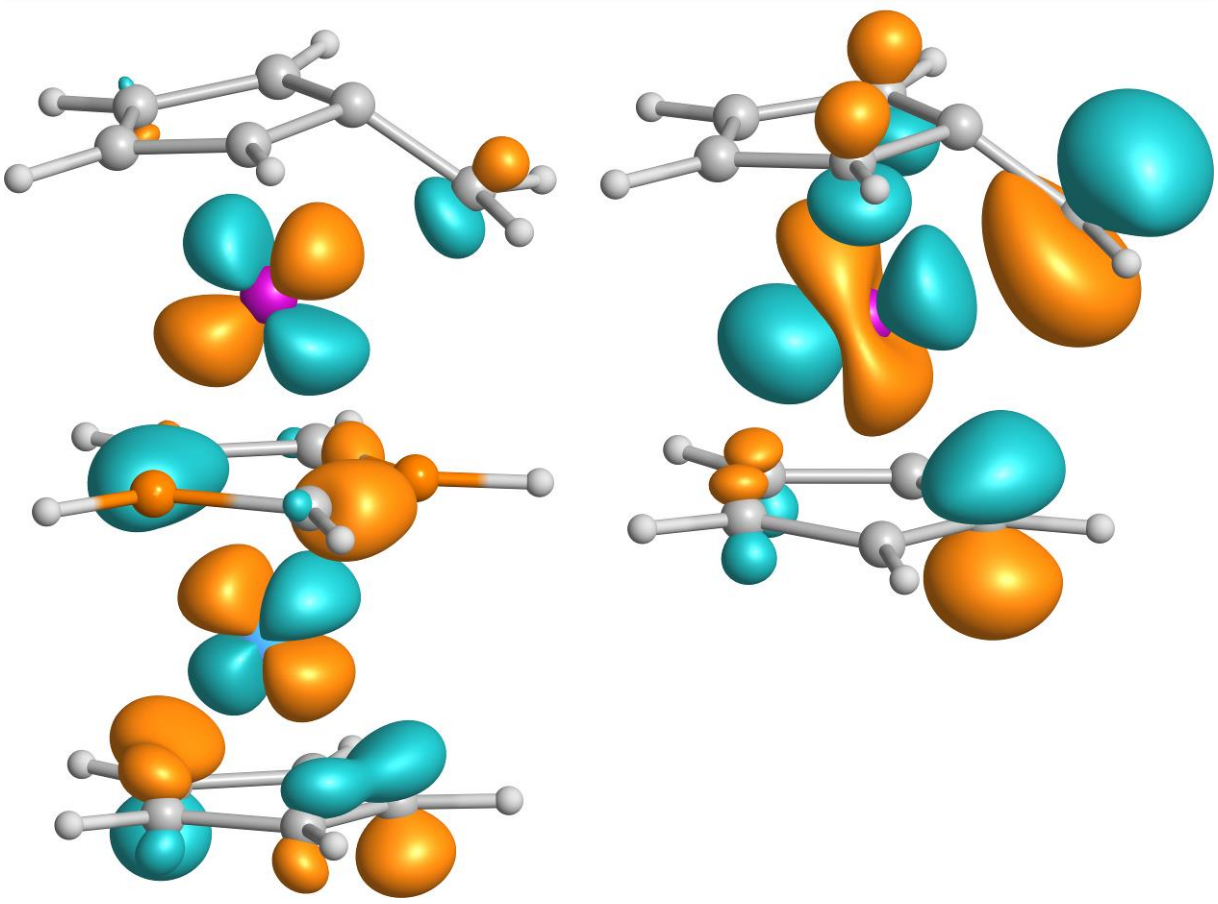

Figure 10. LUMOs of the parent cations **2'** and **3'** at BP86/def2-TZVPP//PBE/L2. MO isodensity surface 0.05.

Conclusion

The first example of the methylium cation with a triple-decker substituent $[CpCo(C_3B_2Me_5)RuC_5Me_4CH_2]^+$ (**2**) has been synthesized while its structure, reactivity, and electrochemistry have been investigated. The reactivity of **2** with various nucleophiles demonstrates reliable and selective two-step functionalization of the triple-decker complexes. A number of the triple-decker derivatives $CpCo(C_3B_2Me_5)RuC_5Me_4CH_2R$ have been synthesized and structurally characterized. Reaction of **2** with the aromatic amines led to the selective formation of the electrophilic substitution products in high yields. X-Ray diffraction data for **2** confirm that the carbenium carbon atom is coordinated to the ruthenium atom and the structure is best described as bearing η^6-fulvene-ruthenium moiety which was also confirmed by DFT calculations. Methylated triple-decker substituent $CpCo(C_3B_2Me_5)RuC_5Me_4$ possesses greater stabilization of the methylium cation by 2.5 kcal mol^{-1} compared to sandwich-type substituent

$Cp^*RuC_5Me_4$ showing a record stabilization of the methylium cation. Spectroelectrochemistry and bulk electrolysis allowed to observe the transformation of the cation **2** into the -CH_2CH_2- bridged triple-decker complex **10** which was also obtained by chemical reduction of **2**.

Experimental Section

All the reactions were carried out under an argon atmosphere, using anhydrous solvents prepared according to standard procedures. The products were isolated in air. Complex **1** was synthesized according to previously described procedure.[14] The ^1H, ^{11}B, ^{13}C, and ^{31}P NMR spectra were recorded on a Bruker Avance-400 (400.13 MHz (^1H), 128.38 MHz (^{11}B), 100.61 MHz (^{13}C), 161.98 MHz (^{31}P)) instrument relative to residual signals of the solvent (^1H, ^{13}C) or $BF_3{\cdot}Et_2O$ and 80% H_3PO_4 (external standards for ^{11}B and ^{31}P, respectively). The IR spectrum of the solid was recorded on a Infralum FT-801 (Lumex) FTIR spectrometer in Nujol mull over the range 400–4000 cm^{-1}.

[CpCo(1,3-$C_3B_2Me_5$)Ru($C_5Me_4CH_2$)]PF_6 (2PF_6): $[CPh_3]PF_6$ (110 mg, 0.284 mmol) was added to a blue solution of **1** (142 mg, 0.288 mmol) in CH_2Cl_2 (5 ml). The color changed immediately to red and the reaction mixture was stirred for 2 h, filtered and product was precipitated by addition of Et_2O. The precipitate formed was separated and washed with Et_2O. After re precipitation with diethyl ether from CH_2Cl_2 and drying *in vacuo* complex **2**PF_6 was obtained as a dark-red air-stable solid. Yield 164 mg (90%). ^1H NMR ($CDCl_3$, 25 ^oC): δ = 4.85 (s, 5H; Cp), 4.55 (s, 2H; CH_2), 2.16 (s, 6H; CMe, C_3B_2), 1.72 (s, 6H, CMe, $C_5Me_4CH_2$), 1.66 (s, 3H, CMe, C_3B_2), 1.23 (s, 6H, CMe, $C_5Me_4CH_2$), 1.13 (br s, 6H, BMe, C_3B_2) ppm; $^{11}B\{^1H\}$ NMR ($CDCl_3$, 25 ^oC): δ = 15.99 (s) ppm; ^{13}C NMR (acetone-d^6, 25 ^oC): δ = 105.8 (s, $\underline{C}_5Me_4$), 98.9 (s, $\underline{C}_5CH_2$), 93.5 (s, $\underline{C}_5Me_4$), 84.7 (dquint, J_{CH} = 181.9 Hz, J^2_{CH} = 6.7 Hz, $\underline{Cp}Co$), 76.2 (t, J_{CH} = 165.9 Hz, $\underline{C}H_2$), 18.4 (q, J_{CH} = 127.9 Hz, $C\underline{C}H_3$), 17.6 (q, J_{CH} = 126.4 Hz, $C\underline{C}H_3$), 9.7 (q, J_{CH} = 129.1 Hz, $C\underline{C}H_3$), 7.9 (q, J_{CH} = 129.1 Hz, $C\underline{C}H_3$) ppm (some signals from carbon atoms were not detected because of interaction with quadruple nuclei of boron); elemental analysis $C_{23}H_{34}B_2CoF_6PRu$ (%): calcd: C 43.36, H 5.38, B 3.39; found: C 43.14, H 5.36, B 3.15. MS (EI): M^+ 493.2.

CpCo(1,3-$C_3B_2Me_5$)Ru($C_5Me_4CH_2OH$) (4): A 15% aqueous KOH solution (10 ml) was poured into the suspension of **2**PF_6 (100 mg, 0.157 mmol) in THF (5 ml) and the resulting two-phase system was stirred for 3 h. The organic phase was separated and evaporated to dryness; residue was taken up in Et_2O and passed through thin layer (ca. 2 cm) of alumina. All volatiles were removed *in vacuo* to give blue solid product. Yield 71 mg (89%). ^1H NMR (acetone-d^6, 25 ^oC): δ = 4.37 (s, 5H; Cp), 3.99 (d, 2H; J = 5.6 Hz, CH_2), 2.19 (s, 6H; CMe, C_3B_2), 1.70 (s, 3H, CMe, C_3B_2), 1.52 (s, 6H, CMe, $C_5Me_4CH_2$), 1.49 (s, 6H, CMe, $C_5Me_4CH_2$), 1.06 (br s, 6H, BMe,

C_3B_2) ppm; $^{11}B\{^1H\}$ NMR (acetone-d^6, 25 °C): δ = 13.68 (s) ppm; $^{13}C\{^1H\}$ NMR (acetone-d^6, 25 °C): δ = 82.6 (s, CpCo), 79.7 (s, (C_5CH_2), 78.4 (s, C_5Me_4), 77.8 (s, C_5Me_4), 57.0 (s, CH_2), 19.7 (s, CCH_3), 18.3 (s, CCH_3), 9.8 (s, CCH_3), 9.7 (s, CCH_3) ppm (some signals from carbon atoms were not detected because of interaction with quadruple nuclei of boron); IR (CaF_2, nujol, cm^{-1}): ν_{OH} = 3255 (br). Elemental analysis $C_{23}H_{35}B_2CoORu$ (%): calcd: C 54.26, H 6.93, B 4.25; found: C 54.44, H 7.05, B 4.11.

[CpCo(1,3-$C_3B_2Me_5$)Ru($C_5Me_4CH_2PPh_3$)]PF_6 (5PF_6): Mixture of **2**PF_6 (100 mg, 0.157 mmol) and PPh_3 (45 mg, 0.171 mmol) in CH_2Cl_2 (4 ml) was stirred for 2 h, then Et_2O (35 ml) wa added. The grayish precipitate was separated, washed with diethyl ether (3 × 10 mL), and drie *in vacuo*. Yield 128 mg (91%). ^1H NMR (acetone-d^6, 25 °C): δ = 7.93 (br t, 3H, *J* = ca. 7 Hz, *p* C_6H_5), 7.76 – 7.63 (overlapping multiplets, 12H, *o*-, *m*-C_6H_5), 4.43 (s, 5H; Cp), 4.12 (d, 2H; J_{P} = 10.8 Hz, CH_2), 2.17 (s, 6H; CMe, C_3B_2), 1.68 (s, 3H, CMe, C_3B_2), 1.45 (s, 6H, CMe, C_5), 1.0 (br s, 6H, BMe, C_3B_2), 0.89 (s, 6H, CMe, C_5) ppm; $^{11}B\{^1H\}$ NMR (acetone-d^6, 25 °C): δ = 13.6 (s) ppm; $^{13}C\{^1H\}$ NMR (acetone-d^6, 25 °C): δ = 135.4 (d, J_{CP} = 2.8 Hz, C_p, PPh_3), 134.9 (d, J_{CP} = 9.7 Hz, C_o or C_m, PPh_3), 130.2 (d, J_{CP} = 11.9 Hz, C_o or C_m, PPh_3), 117.9 (d, J_{CP} = 80.4 Hz, C_{ipso} PPh_3), 82.8 (s, CpCo), 80.3 (s, C_5Me_4), 77.9 (s, C_5Me_4), 69.7 (s, C_5CH_2), 25.3 (d, J_{CP} = 43.2 Hz CH_2), 19.3 (s, CCH_3), 18.0 (s, CCH_3), 10.3 (s, CCH_3), 9.6 (s, CCH_3) ppm (some signals fron carbon atoms were not detected because of interaction with quadruple nuclei of boron); $^{31}P\{^1H$ NMR (acetone-d^6, 25 °C): δ = 14.54 (s, PPh_3), –144.24 (septet, J_{PF} = 707 Hz, PF_6) ppm elemental analysis $C_{41}H_{49}B_2CoF_6P_2Ru$ (%): calcd: C 54.75, H 5.49, B 2.40; found: C 54.70, H 5.30, B 2.20.

[CpCo(1,3-$C_3B_2Me_5$)Ru($C_5Me_4CH_2NEt_3$)]PF_6 (6PF_6): NMR-tube experiment: NEt_3 (5 mg 0.049 mmol) was added to the solution of **2**PF_6 (25 mg, 0.039 mmol) in acetone-d^6 (0.5 ml contains ca. 5 vol. % of water). The solution immediately became purple. ^1H NMR (acetone-d^6 25 °C) for **6PF_6**: δ = 4.46 (s, 5H; Cp), 4.06 (s, 2H, CH_2), 3.37 (quart, 6H, $N(CH_2CH_3)_3$, *J* = 9.(Hz), 2.17 (s, 6H; CMe, C_3B_2), 1.69 (overlapping singlets, 9H, 3H from CMe, C_3B_2 and 6H fron CMe, C_5), 1.55 (s, 6H, CMe, C_5), 1.31 (br t, 9H, *J* = ca. 8 Hz, $N(CH_2CH_3)_3$), 1.04 (br s, 6H BMe, C_3B_2) ppm.

CpCo(1,3-$C_3B_2Me_5$)Ru($C_5Me_4CH_2OCH_2C_5Me_4$)Ru(1,3-$C_3B_2Me_5$)CoCp (7): The NMR-tub from previous experiment was left for 3 days, after which the color changed on blue and the blue crystals of the complex **7** were formed. The crystals were separated and washed with 1 ml of hexane. Yield 16 mg (80%). ^1H NMR (CD_2Cl_2, 25 °C): δ = 4.25 (s, 10H, 2Cp), 3.78 (s, 4H, CH_2, (Ru)C_5), 2.12 (s, 12H, 4CMe, C_3B_2), 1.77 (s, 6H, 2CMe, C_3B_2), 1.46 (s, 12H, 4CMe, (Ru)C_5), 1.42 (s, 12H, 4CMe, (Ru)C_5), 1.05 (s, 12H, 4BMe, C_3B_2) ppm; $^{11}B\{^1H\}$ NMR (CD_2Cl_2, 25 °C):

δ = 13.95 (s) ppm; elemental analysis $C_{46}H_{68}B_4Co_2ORu_2$ (%): calcd: C 55.23, H 6.85, B 4.32; found: C 55.37, H 6.92, B 4.28.

[CpCo(1,3-$C_3B_2Me_5$)Ru($C_5Me_4CH_2$(4-$C_6H_4NEt_2H$)]PF_6 (8PF_6): $PhNEt_2$ (15 mg, 0.107 mmol) was added to the solution of **2**PF_6 (64 mg, 0.1 mmol) in acetone (1 ml), then it was stirred overnight, after which hexane (15 ml) was added. The blue-gray precipitate was separated, washed with diethyl ether (3 × 5 mL), and dried in vacuo. Yield 65 mg (83%). ^{1}H NMR (CD_2Cl_2, 25 ^{o}C): δ = 7.43 (d, 2H, AA'BB', J_{AB} = ca. 7.6 Hz, *p*-C_6H_4), 7.31 (d, 2H, AA'BB', J_{AB} = ca. 7.6 Hz, *p*-C_6H_4), 4.67 (s, 5H; Cp), 3.62 (quart, 4H, *J* = 7.2 Hz, N($C\underline{H}_2CH_3)_2$), 3.24 (s, 2H CH_2), 1.99 (s, 6H; CMe, C_3B_2), 1.84 (s, 6H, CMe, C_5), 1.77 (s, 6H, CMe, C_5), 1.30 (overlapping singlets, 9H, 3H from C$\underline{Me}$, C_3B_2 and 6H from BMe, C_3B_2), 1.21 (t, 6H, *J* = 7.2 Hz N($CH_2C\underline{H}_3)_2$) ppm; ^{11}B{^{1}H} NMR (CD_2Cl_2, 25 ^{o}C): δ = 13.05 (s) ppm; elemental analysis $C_{33}H_{49}B_2CoF_6NPRu$ (%): calcd: C 50.41, H 6.28, B 2.75; found: C 50.67, H 6.41, B 2.55.

In a similar experiment, an NMR tube was charged with complex **2**PF_6 (6.4 mg, 0.01 mmol), a d^6-acetone (0.5 ml) and $PhNEt_2$ (1.8 mg, 0.012 mmol, 20% excess). ^{1}H NMR spectra were recorded and it was found that after 24 h the resonances of the starting material **2**PF_6 completely disappeared. In a related experiment, the NMR tube was charged with cation **3**PF_6 (5.1 mg, 0.01 mmol), a d^6-acetone (0.5 ml) and $PhNEt_2$ (1.7 mg, 0.012 mmol, 14% excess). The disappearance of the resonances for **3**PF_6 was observed after 8 h.

2-(CpCo(1,3-$C_3B_2Me_5$)Ru($C_5Me_4CH_2$)(4-$MeC_6H_3NH_2$) (9): 4-$MeC_6H_4NH_2$ (32 mg, 0.3 mmol) was added to the solution of **2**PF_6 (64 mg, 0.1 mmol) in acetone (1 ml), then it was stirred overnight. Chromatography on alumina column (0.5×20 cm) with petroleum ether gave blue band. All volatiles were removed in vacuo giving blue solid, which was dried in vacuo. Yield 43 mg (71%). ^{1}H NMR ($CDCl_3$, 25 ^{o}C): δ = 6.74 (d, 1H, *J* = 7.6 Hz, $C_6\underline{H}_3$), 6.52 (d, 1H, *J* = 7.6 Hz $C_6\underline{H}_3$), 6.36 (s, 1H, $C_6\underline{H}_3$), 4.23 (s, 5H; Cp), 3.49 (br s, 2H, NH_2), 3.10 (s, 2H, CH_2), 2.16 (s, 6H CMe, C_3B_2), 2.08 (s, 3H, CH_3), 1.69 (s, 3H, CMe, C_3B_2), 1.51 (s, 6H, CMe, C_5), 1.39 (s, 6H CMe, C_5), 1.05 (br s, 6H, BMe, C_3B_2) ppm; ^{11}B{^{1}H} NMR ($CDCl_3$, 25 ^{o}C): δ = 14.21 (s) ppm elemental analysis $C_{30}H_{42}B_2CoNRu$ (%): calcd: C 60.23, H 7.08, B 3.61; found: C 60.37, H 7.35 B 3.51.

CpCo(1,3-$C_3B_2Me_5$)Ru($C_5Me_4CH_2CH_2C_5Me_4$)Ru(1,3-$C_3B_2Me_5$)CoCp (**10**): Suspension of **2**PF_6 (100 mg, 0.157 mmol) and Zn (40 mg, 0.628 mmol) in 5 ml of THF was stirred for 24 h. The reaction mixture was evaporated to dryness with small amount of alumina. Chromatography on alumina (2×20 cm) with light petroleum (b.p. 40-60 ^{o}C) gave two blue bands. Evaporation of the first gave traces of blue complex **1** (3 mg) and the second gave blue complex **10**. Yield 72 mg (91%). ^{1}H NMR ($CDCl_3$, 25 ^{o}C): δ = 4.16 (s, 10H, 2Cp), 2.06 (s, 12H, 4CMe, C_3B_2), 1.75 (s, 4H, CH_2, (Ru)C_5), 1.58 (s, 6H, 2CMe, C_3B_2), 1.43 (s, 12H, 4CMe, (Ru)C_5), 1.33 (s, 12H, 4CMe,

(Ru)C_5), 0.95 (s, 12H, 4BMe, C_3B_2) ppm; $^{11}B\{^1H\}$ NMR ($CDCl_3$, 25 ^oC): δ = 14.27 (s) ppm; $^{13}C\{^1H\}$ NMR ($CDCl_3$, 25 ^oC): δ = 81.8 (s, CoCp), 80.9 (s, C_q-Ru(C_5)), 80.6 (s, C_q-Ru(C_5)), 77.1 (s, C_q-Ru(C_5)), 26.1 (s, CH_2), 19.6 (s, CCH_3), 18.4 (s, CCH_3), 10.2 (s, CCH_3), 10.1 (s, CCH_3) ppm (some signals from carbon atoms were not detected because of interaction with quadruple nucleus of boron); elemental analysis $C_{46}H_{68}B_4Co_2Ru_2$(%): calcd: C 55.97, H 6.95, B 4.47; found: C 56.13, H 7.20, B 4.64.

X-Ray Crystallography. X-ray diffraction experiments were carried out with a Bruker SMART APEX2 CCD area detector, using graphite monochromated $Mo_{K\alpha}$ radiation (λ = 0.71073 Å,) a 100 K.[22] The structures were solved by direct method and refined by the full-matrix least squares technique against F^2 in anisotropic approximation for non-hydrogen atoms. All hydroge atoms were refined in isotropic approximation in riding model. The absorption correction wa applied semi-empirically using SADABS program. All calculations were performed usin SHELXTL 5.1.[23]

Crystals of **2**PF_6 were grown up by slow diffusion in the two-layer system Et_2O/CH_2Cl_2 Crystallographic data for **2**PF_6: $C_{23}H_{34}B_2CoF_6PRu$, M_r = 637.09, 0.42 × 0.25 × 0.13 mm monoclinic, space group $P2_1/n$, a = 17.009(3), b = 16.515(3), c = 27.246(5) Å, β = 94.430(3)°, V = 7631(2) Å^3, Z = 12, d_{calc} = 1.664 Mg m^{-3}, $\mu(Mo_{K\alpha})$ = 1.363 mm^{-1}, T = 100(2) K, $2\theta_{max}$ = 58° 101823 reflections measured, 18411 independent (R_{int} = 0.0545), $R1$ = 0.0504 (14366 reflection with $I > 2\sigma(I)$), wR_2 = 0.1418 (all data), T_{max}/T_{min} = 0.842/0.598, GOF = 1.025, max. res. densit peaks: 1.30 to –1.21 e Å^{-3}. Compound **2**PF_6 crystallizes with three independent molecules in th unit cell. Mutual orientation of the five-membered rings in all independent molecules of **2**PF vary between eclipsed and staggered conformation.

Crystals of **4** were grown up by slow evaporation of hexane solution. Crystallographic data for **4** $C_{23}H_{35}B_2CoORu$, M_r = 509.13, 0.45 × 0.22 × 0.20 mm, tetragonal, $I4_1/a$, a = 32.5131(10) Å, b = 32.5131(10) Å, c = 8.6384(6) Å, V = 9131.7(7) Å^3, Z = 16, d_{calc} = 1.481 Mg m^{-3}, $\mu(Mo_{K\alpha})$ = 1.399 mm^{-1}, T = 100(2) K, $2\theta_{max}$ = 61°, 20155 reflections measured, 6981 independent (R_{int} = 0.0346), $R1$ = 0.029 (5780 reflections with $I > 2\sigma(I)$), wR_2 = 0.0730 (all data), T_{max}/T_{min} = 0.751/0.691, GOF = 1.023, max. res. density peaks: 0.79 to –0.40 e Å^{-3}. The hydrogen atom o the OH group was found in Fourier synthesis and refined isotropically.

Crystals of **7** were grown up by slow crystallization of acetone solution. Crystallographic data for **7**: $C_{46}H_{68}B_4Co_2ORu_2$, M_r = 1000.24, 0.41 × 0.28 × 0.10 mm, monoclinic, space group $P2_1/c$, a = 18.1040(9) Å, b = 15.2435(8) Å, c = 17.4914(9) Å, β = 105.9430(10)°, V = 4641.4(4) Å^3, Z = 4, d_{calc} = 1.431 Mg m^{-3}, $\mu(Mo_{K\alpha})$ = 1.373 mm^{-1}, T = 100(2) K, $2\theta_{max}$ = 56°, 24621 reflections measured, 11156 independent (R_{int} = 0.0294), $R1$ = 0.0300 (8956 reflections with $I > 2\sigma(I)$), wR_2

= 0.0758 (all data), T_{max}/T_{min} = 0.8749/0.6029, GOF = 0.994, max. res. density peaks: 0.72 to –0.67 e Å^{-3}.

Crystals of **8**PF_6 were grown up by slow evaporation of acetone solution. Crystallographic data for **8**PF_6: $C_{33}H_{49}B_2CoNRu\cdot 0.25$ acetone, M_r = 800.84, 0.50 × 0.22 × 0.12 mm, triclinic, space group *P-1*, a = 8.637(2) Å, b = 16.933(5) Å, c = 26.940(7) Å, α = 76.318(4)°, β = 83.410(4)°, γ = 88.085(4)°, V = 3802.80(17) Å^3, Z = 4, d_{calc} = 1.399 Mg m^{-3}, μ(Mo$_{K\alpha}$) = 0.929 mm^{-1}, T = 100(2) K, $2\theta_{max}$ = 52°, 24332 reflections measured, $R1$ = 0.0781 (16852 reflections with $I > 2\sigma(I)$), wR_2 = 0.2134 (all data), T_{max}/T_{min} = 0.896/0.653, GOF = 1.045, max. res. density peaks: 2.50 to –1.0 e Å^{-3}. Compound **8**PF_6 crystallizes with two independent molecules in the unit cell. Crystal o **8**PF_6 was found to be twinned and refined with HKLF 5 (BASF = 0.480).

Crystals of **9** were grown up by slow evaporation of hexane solution. Crystallographic data for **9** $C_{30}H_{42}B_2CoNRu$, M_r = 598.27, 0.15 × 0.13 × 0.06 mm, monoclinic, space group *P2₁/c*, a = 11.387(7) Å, b = 28.64(2) Å, c = 8.528(6) Å, β = 100.36(2)°, V = 2736(3) Å^3, Z = 4, d_{calc} = 1.45 Mg m^{-3}, μ(Mo$_{K\alpha}$) = 1.178 mm^{-1}, T = 100(2) K, $2\theta_{max}$ = 56°, 30396 reflections measured, 660 independent (R_{int} = 0.0825), $R1$ = 0.0452 (4626 reflections with $I > 2\sigma(I)$), wR_2 = 0.1017 (al data), T_{max}/T_{min} = 0.932/0.843, GOF = 1.026, max. res. density peaks: 0.57 to –0.75 e Å^{-3}.

Crystals of **10** were grown up by slow evaporation of hexane/acetone solution (2/1) Crystallographic data for **10**: $C_{46}H_{68}B_4Co_2Ru_2$, M_r = 984.24, 0.60 × 0.14 × 0.13 mm, monoclinic space group *P2₁/n*, a = 8.5454(4) Å, b = 19.5013(9) Å, c = 13.6860(6) Å, β = 99.7160(10)°, V = 2248.01(18) Å^3, Z = 2, d_{calc} = 1.454 Mg m^{-3}, μ(Mo$_{K\alpha}$) = 1.414 mm^{-1}, T = 100(2) K, $2\theta_{max}$ = 56° 29816 reflections measured, 5420 independent (R_{int} = 0.0238), $R1$ = 0.0187 (5095 reflection with $I > 2\sigma(I)$), wR_2 = 0.0495 (all data), T_{max}/T_{min} = 0.840/0.484, GOF = 1.060, max. res. density peaks: 0.46 to –0.29 e Å^{-3}. Compound **10** crystallizes with molecules lying acros crystallographic inversion centers.

Electrochemistry and spectroelectrochemistry. Anhydrous 99.9% dichloromethane was a Aldrich product. Fluka [NBu_4][PF_6] (electrochemical grade) was used as supporting electrolyt (0.2 M). Cyclic voltammetry was performed in a three-electrode cell containing a platinun working electrode surrounded by a platinum-spiral counter electrode, and an aqueous saturate calomel reference electrode (SCE) mounted with a Luggin capillary. For low-temperature measurements, the central part of the cell (nonisothermal assembly) was enclosed by a thermostatic jacket through which a cooled liquid was circulated. At room temperature the reference electrode was an aqueous saturated calomel electrode (SCE); at low temperature, a Ag/AgCl electrode, filled with the solution under investigation, was used. BAS 100W electrochemical analyzer was used as polarizing unit. All the potential values are referred to the saturated calomel electrode (SCE). Under the present experimental conditions, the one-electron

oxidation of ferrocene occurs at $E°'$=+0.39 V. Controlled potential coulometry was performed in an H-shaped cell with anodic and cathodic compartments separated by a sintered-glass disk. The working macroelectrode was a platinum gauze; a mercury pool was used as the counter electrode. The UV-vis spectroelectrochemical measurements were carried out using a Perkin-Elmer Lambda 900 UVvis spectrophotometer and an OTTLE (optically transparent thin-layer electrode) cell[24] equipped with a Pt-minigrid working electrode (32 wires/cm), Pt minigrid auxiliary electrode, Ag wire pseudoreference and CaF_2 windows. The electrode potential was controlled during electrolysis by an Amel potentiostat 2059 equipped with an Amel function generator 568. Nitrogen-saturated solutions of the compound under study were used with $[NBu_4][PF_6]$ (0.2 M) as supporting electrolyte. Working potential was initially set ~200 mV higher (on reduction) or lower (on oxidation) than the peak potential of the process under study and spectra were progressively collected by increasing or decreasing the potential by step of 50 mV (2 min electrolysis).

Computational Details:

Geometry optimizations were performed without constraints using PBE exchange correlation functional,[25],[26] the scalar-relativistic Hamiltonian,[27] atomic basis sets of generally contracted Gaussian functions,[28] and a density-fitting technique[29] as implemented in a recent version of Priroda code.[30] The all-electron triple-ζ basis set L2 (close to cc-pVTZ)[31] augmented by two polarization functions was used.[32] Frequency calculations were performed at the same level of theory.

Mayer bond orders [33] were calculated using BP86 functional and triple-ζ basis set augmented by two polarization functions def2-TZVPP[34] with the help of the Gaussian 09[35] and Chemissian[36] programs. The ChemCraft software[37] was used for molecular modeling and visualization.

Supporting Information

Supporting information (SI) available for electrochemistry, Table S1 and S2 with bond length and angles, and computational details. CCDC numbers CCDC-1547981 (**2**), 1547985 (**4**), 1547983 (**7**), 1547980 (**8**), 1547984 (**9**), and 1547982 (**10**) contain the supplementary crystallographic data for this paper. These data can be obtained free of charge from The Cambridge Crystallographic Data Centre via www.ccdc.cam.ac.uk/data_request/cif. For SI and crystallographic data in CIF or other electronic format see DOI: XX.XXX/XXXX.

Footnotes

* Corresponding authors: muratov@ineos.ac.ru, asromanov5@gmail.com, fabrizi@unisi.it, walter.siebert@uni-heidelberg.de

Current affiliation for Dr. Alexander S. Romanov: University of East Anglia, Earlham Road, Norwich, NR4 7TJ, UK

References

[1] M. W. Crofton, W. A. Kreiner, M.-F. Jagod, B. D. Rehfuss, T. Oka, *J. Chem. Phys.*, **1985**, *83*, 3702–3703, and references therein.

[2] G. A. Olah, E. B. Baker, J. C. Evans, W. S. Tolgyesi, J. S. McIntyre, I. J. Bastien, *J. Am Chem. Soc.*, **1964**, *86*, 1360–1373.

[3] J. March, *Advanced Organic Chemistry. Reactions, Mechanisms and Structure*. 4th Ed. Wiley, New York, **1992**.

[4] R. E. Davis, H. D. Simpson, N. Conte, R. Pettit, *J. Am. Chem. Soc.*, **1971**, *93*, 6688–6690.

[5] (a) W. S. Trahanovsky, D. K. Wells, *J. Am. Chem. Soc.*, **1969**, *91*, 5870–5871;

(b) for review see: Watts, W. E. in: Wilkinson, G.; Stone, F. G. A.; Abel E. W. (Eds.) *Comprehensive Organometallic Chemistry*, vol. 8, Pergamon Press, Oxford, **1982**, pp. 1013-1071.

[6] (a) K. M. Nicholas, R. Pettit, *Tetrahedron Lett.*, **1971**, *37*, 3475–3478;

(b) for review see: K. M. Nicholas, *Acc. Chem. Res.*, **1987**, *20*, 207–214.

[7] M. V. Galakhov, V. I. Bakhmutov, I. V. Barinov, O. A.Reutov, *J. Organomet. Chem.*, **1991** *421*, 65–73.

[8] (a) D. Seyferth, C. S. Eschbach, M. O. Nestle, *J. Organomet. Chem.*, **1975**, *97*, C11–C15;

(b) for review see: D. Seyferth, *Adv. Organomet. Chem.*, **1976**, *14*, 97–144.

[9] J. H. Richards, E. A. Hill, *J. Am. Chem. Soc.*, **1959**, *81*, 3484–3485.

[10] For reviews see: (a) W. E. Watts, *J. Organomet. Chem. Library*, **1979**, *7*, 399–459;

(b) see ref. 5b; (c) A. A. Koridze, *Russ. Chem. Rev.*, **1986**, *55*, 277–302;

(d) R. Gleiter, C. Bleiholder, F. Rominger, *Organometallics*, **2007**, *26*, 4850–4859;

(e) C. Bleiholder, F. Rominger, R. Gleiter, *Organometallics*, **2009**, *28*, 1014–1017.

[11] S. Barlow, A. Cowley, J. C. Green, T. J. Brunker, T. Hascall, *Organometallics*, **2001**, *20*, 5351–5359.

[12] (a) R. Gleiter, R. Seeger, *Helv. Chim. Acta*, **1971**, *54*, 1217–1220;

(b) see ref. 10d.

[13] For reviews see: (a) W. Siebert, *Angew. Chem. Int. Ed. Engl.*, **1985**, *24*, 943–958;

(b) W. Siebert, *Pure and Appl. Chem.*, **1988**, *60*, 1345–1348;

(c) Siebert, W. *Adv. in Organomet. Chem.*, **1993**, *35*, 187–210.

[14] W. Siebert, A. R. Kudinov, P. Zanello, M. Yu. Antipin, V. V. Scherban, A. S. Romanov, D. V. Muratov, Z. A. Starikova, M. Corsini, *Organometallics*, **2009**, *28*, 2707–2715.

[15] D. V. Muratov, A. S. Romanov, T. V. Timofeeva, W. Siebert, M. Corsini, S. Fedi, P. Zanello, A. R. Kudinov, *Organometallics*, **2013**, *32*, 2713–2724.

[16] (a) U. Köelle, J. Grub, *J. Organomet. Chem.*, **1985**, *289*, 133–139;

(b) A. Z. Kreindlin, P. V. Petrovskii, M. I. Rybinskaya, A. I. Yanovsky, Yu. T. Struchkov, *J. Organomet. Chem.*, **1987**, *319*, 229–237;

(c) A. I. Yanovsky, Yu. T. Struchkov, A. Z. Kreindlin, M. I. Rybinskaya, *J. Organomet. Chem.* **1989**, *369*, 125–130.

[17] For review see: A. Z. Kreindlin, M. I. Rybinskaya, *Russ. Chem. Rev.*, **2004**, *73*, 417–432.

[18] D. V. Muratov, A. S. Romanov, A. R. Kudinov, *Mendeleev Commun*., **2015**, *25*, 109–110.

[19] For the conformation analysis of the ruthenocene-type complexes, see:

(a) S. Carter, J.N. Murrell, *J. Organomet. Chem.*, **1980**, *192*, 399–408 and references therein;

(b) I.E. Zanin, M.Yu. Antipin, *Crystallography Reports*, **2003**, *48*, 249–258. Translated from *Kristallografiya*, **2003**, *48*, 283–292.

[20] In Electrochemistry and Spectroelectrochemistry section compound numbers are given in brackets with charges, e.g. $[\mathbf{3}]^0$ and $[\mathbf{3}]^+$.

[21] DFT calculations were performed for the eclipsed conformation which is the most thermodynamically stable for the ruthenocene-type sandwich complexes.

[22] *APEX2 software package*, Bruker AXS Inc., Madison, WI, USA, **2005**.

[23] G. M. Sheldrick, *SHELXTL v. 5.10, Structure Determination Software Suite*, Bruker AXS Inc., Madison, WI, USA, **1998**.

[24] M. Krejčik, M. Daněk, F. Hartl, *J. Electroanal. Chem.*, **1991**, *317*, 179–187.

[25] J. P. Perdew, K. Burke, M. Ernzerhof, *Phys. Rev. Lett.*, **1996**, *177*, 3865–3868.

[26] A. D. Becke, *Phys. Rev. A*, **1988**, *38*, 3098–3100.

[27] K. G. Dyall, *J. Chem. Phys.*, **1994**, *100*, 2118–2127.

[28] D. N. Laikov, *Chem. Phys. Lett.*, **2005**, *416*, 116–120.

[29] D. N. Laikov, *Chem. Phys. Lett.*, **1997**, *281*, 151–156.

[30] D. N. Laikov, Yu. A. Ustynyuk, *Izv. Akad. Nauk, Ser. Khim.*, **2005**, 804–810; *Russ. Chem. Bull.*, **2005**, 54, 820–826 (*Engl. Transl.*).

[31] T. H. Dunning, Jr., *J. Chem. Phys.*, **1989**, *90*, 1007–1023.

[32] E. Ya. Misochko, A. V. Akimov, V. A. Belov, D. A. Tyurin, D. N. Laikov, *J. Chem. Phys.*, **2007**, *127*, 084301.

10.1002/chem.201702571

[33] I. Mayer, I. *Chem. Phys. Lett.*, **1983**, *97*, 270–274.

[34] F. Weigend, R. Ahlrichs, *Phys. Chem. Chem. Phys.*, **2005**, *7*, 3297–3305.

[35] M. J. Frisch, G. W. Trucks, H. B. Schlegel, G. E. Scuseria, M. A. Robb, J. R. Cheeseman, G. Scalmani, V. Barone, B. Mennucci, G. A. Petersson, H. Nakatsuji, M. Caricato, X. Li, H. P. Hratchian, A. F. Izmaylov, J. Bloino, G. Zheng, J. L. Sonnenberg, M. Hada, M. Ehara, K. Toyota, R. Fukuda, J. Hasegawa, M. Ishida, T. Nakajima, Y. Honda, O. Kitao, H. Nakai, T. Vreven, J. A. Montgomery, Jr., J. E. Peralta, F. Ogliaro, M. Bearpark, J. J. Heyd, E. Brothers, K. N. Kudin, V. N. Staroverov, R. Kobayashi, J. Normand, K. Raghavachari, A. Rendell, J. C Burant, S. S. Iyengar, J. Tomasi, M. Cossi, N. Rega, J. M. Millam, M. Klene, J. E. Knox, J. B Cross, V. Bakken, C. Adamo, J. Jaramillo, R. Gomperts, R. E. Stratmann, O. Yazyev, A. J Austin, R. Cammi, C. Pomelli, J. W. Ochterski, R. L. Martin, K. Morokuma, V. G. Zakrzewski G. A. Voth, P. Salvador, J. J. Dannenberg, S. Dapprich, A. D. Daniels, O. Farkas, J. B Foresman, J. V. Ortiz, J. Cioslowski, D. J. Fox, *Gaussian 09, Revision A.02*, Gaussian, Inc. Wallingford, USA, **2009**.

[36] L. Skripnikov, *Chemissian 2.200*, **2011**, http://chemissian.com.

[37] G. A. Zhurko, *ChemCraft 1.6*, **2011**, http://www.chemcraftprog.com.